

## Orbit

The International Journal on Orbital Disorders, Oculoplastic and  
Lacrimal Surgery

ISSN: (Print) (Online) Journal homepage: [informahealthcare.com/journals/iorb20](https://informahealthcare.com/journals/iorb20)

# Functional and molecular 3D mapping of angiosarcoma tumor using non-invasive laser speckle, hyperspectral, and photoacoustic imaging

Magne Stridh, Ulf Dahlstrand, Magdalena Naumovska, Karl Engelsberg,  
Bodil Gesslein, Rafi Sheikh, Aboma Merdasa & Malin Malmsjö

To cite this article: Magne Stridh, Ulf Dahlstrand, Magdalena Naumovska, Karl Engelsberg,  
Bodil Gesslein, Rafi Sheikh, Aboma Merdasa & Malin Malmsjö (09 Apr 2024): Functional and  
molecular 3D mapping of angiosarcoma tumor using non-invasive laser speckle, hyperspectral,  
and photoacoustic imaging, Orbit, DOI: [10.1080/01676830.2024.2331718](https://doi.org/10.1080/01676830.2024.2331718)

To link to this article: <https://doi.org/10.1080/01676830.2024.2331718>



© 2024 The Author(s). Published with  
license by Taylor & Francis Group, LLC.



Published online: 09 Apr 2024.



Submit your article to this journal [↗](#)



Article views: 239



View related articles [↗](#)



View Crossmark data [↗](#)

# Functional and molecular 3D mapping of angiosarcoma tumor using non-invasive laser speckle, hyperspectral, and photoacoustic imaging

Magne Stridh , Ulf Dahlstrand , Magdalena Naumovska , Karl Engelsberg , Bodil Gesslein, Rafi Sheikh , Aboma Merdasa , and Malin Malmsjö 

Department of Clinical Sciences Lund, Ophthalmology, Lund University, Lund, Sweden

## ABSTRACT

**Purpose:** The gold standard for skin cancer diagnosis is surgical excisional biopsy and histopathological examination. Several non-invasive diagnostic techniques exist, although they have not yet translated into clinical use. This is a proof-of-concept study to assess the possibility of imaging an angiosarcoma in the periocular area.

**Methods:** We use laser speckle, hyperspectral, and photoacoustic imaging to monitor blood perfusion and oxygen saturation, as well as the molecular composition of the tissue. The information obtained from each imaging modality was combined in order to yield a more comprehensive picture of the function, as well as molecular composition of a rapidly growing cutaneous angiosarcoma in the periocular area.

**Results:** We found an increase in perfusion coupled with a reduction in oxygen saturation in the angiosarcoma. We could also extract the molecular composition of the angiosarcoma at a depth, depicting both the oxygen saturation and highlighting the presence of connective tissue via collagen.

**Conclusions:** We demonstrate the different physiological parameters that can be obtained with the different techniques and how these can be combined to provide detailed 3D maps of the functional and molecular properties of tumors useful in preoperative assessment.

## ARTICLE HISTORY

Received 28 December 2023  
Accepted 12 March 2024

## KEYWORDS

Perfusion & oxygenation monitoring; hyperspectral imaging; laser speckle contrast imaging; photoacoustic imaging; angiosarcoma

## Introduction

Skin cancer is one of the most common forms of cancer and is overrepresented around the eyes. The gold standard for the diagnosis and treatment of skin cancer is surgical excisional biopsy and histopathological examination.<sup>1,2</sup> Patients in which tumor excision is found to be non-radical must undergo a second surgical procedure to increase the surgical margin. However, it is especially important in the periorbital area that excision is not more extensive than necessary, in order to preserve the function of the eyelids and protect the eye. If it were possible to delineate the tumor perioperatively, it would be possible to remove the whole tumor in the first surgical intervention, avoiding the need for multiple surgeries.

Various non-invasive imaging techniques have been developed, but each of them has shortcomings.<sup>3–5</sup> For example, dermatoscopy is a visual assessment technique with low resolution, while confocal microscopy and optical coherence tomography have high resolution, but limited depth (0.1–0.2 mm and 1–2 mm,

respectively). Clinical ultrasound can be used to generate images deeper in the tissue, but the resolution is poor. Magnetic resonance imaging has functional imaging capability, but the spatial resolution is low when using acquisition times and magnetic coils suitable in the clinical setting.<sup>6</sup>

State-of-the-art non-invasive biomedical imaging techniques are being developed that can map functional and molecular properties of the tissue surface, sometimes even in three dimensions. Laser speckle contrast imaging (LSCI), developed by Yamamoto et al. in 1993,<sup>7</sup> can be used to assess microcirculation. The area of interest is illuminated with near-infrared (NIR) monochromatic laser light, and interference of the diffusely backscattered light from the illuminated tissue area results in dark and bright areas, a so-called speckle pattern. Analysis of the variations in the speckle pattern provides a measure of the degree of motion in the tissue, which is in part interpreted as the movement of red blood cells, i.e. blood perfusion. LSCI has proven successful in the non-invasive mapping of perfusion in various ophthalmological pathologies including

**CONTACT** Malin Malmsjö  malin.malmsjo@med.lu.se  Skåne University Hospital, Ögonklinik A, admin, 2nd floor, Kioskgatan 1, Lund 221 85, Sweden

© 2024 The Author(s). Published with license by Taylor & Francis Group, LLC.

This is an Open Access article distributed under the terms of the Creative Commons Attribution License (<http://creativecommons.org/licenses/by/4.0/>), which permits unrestricted use, distribution, and reproduction in any medium, provided the original work is properly cited. The terms on which this article has been published allow the posting of the Accepted Manuscript in a repository by the author(s) or with their consent.

glaucoma, retinopathy, and macular degeneration, and has also shown promise as a potential method of monitoring perfusion in the periocular area during reconstructive surgery.<sup>8,9</sup> It has recently attracted attention as a means of detecting changes in perfusion in skin cancers such as malignant melanoma and cherry angioma.<sup>10</sup>

Hyperspectral imaging (HSI) is an emerging technology in which the tissue is illuminated with incandescent light with a broad wavelength range, typically in the NIR range, and thus has the capability to map tissue oxygenation with a high spatial resolution.<sup>11,12</sup> Oxygenated (HbO<sub>2</sub>) and deoxygenated (HbR) hemoglobin absorb light differently, allowing the oxygen saturation (sO<sub>2</sub>) to be calculated and presented in a 2D pixel-by-pixel map. The spectral resolution of HSI also enables the discrimination of healthy skin from skin cancer by mapping the chromophores in the tissue.<sup>13</sup> HSI has hitherto been developed in animal models to monitor oxygen saturation in skin, for example, after radiation exposure<sup>14</sup> or burn trauma,<sup>15</sup> and in raised skin flaps.<sup>16</sup> Although HSI has not yet been implemented clinically, it has been used to evaluate microcirculatory changes in diabetic foot ulcers<sup>17,18</sup> and in peripheral arterial disease,<sup>19</sup> to identify cutaneous artery perforators for microvascular surgery<sup>20</sup> and to monitor cutaneous blood perfusion changes after the injection of local anesthetics during surgery.<sup>11</sup>

Photoacoustic imaging (PAI) is currently one of the most rapidly developing non-invasive biomedical imaging techniques. It is a novel hybrid imaging technology that combines the strengths of optical and ultrasound imaging, and provides high-resolution 3D images of the molecular composition of the tissue at depth.<sup>21</sup> The tissue is irradiated with pulsed laser light, which causes so-called thermoelastic expansion, which in turn generates mechanical waves that can be detected by an ultrahigh-frequency ultrasound scanner. The technique provides a spectral signature of the tissue spatially resolved at a depth. PAI is thus superior to other techniques in the detection of small variations in tissue composition with depth. PAI has shown promising results in the examination of the spectral properties of healthy tissue and its differentiation from basal cell carcinoma, squamous cell carcinoma, and malignant melanoma.<sup>22</sup>

The clinical applicability of LSCI, HSI and PAI for skin tumor diagnostics has been demonstrated in various studies. However, in this study, we assess, for the first time, the combination of these three modalities to map blood perfusion and tissue oxygenation, and to characterize the molecular composition of a skin tumor.

## Methods

### Ethics

The experimental protocol for this study was approved by the Ethics Committee at Lund University, Sweden. The research adhered to the tenets of the Declaration of Helsinki as amended in 2008. Prior to surgery, the patient was given verbal and written information about the study, and the voluntary nature of participation. Informed written consent was obtained and the data were anonymized.

### Patient and lesion characteristics

An 82-year-old woman presented with a redness in the lower left eyelid in the medial canthal area, in 2021. A punch biopsy and computed tomography of the head and orbit were performed. The biopsy showed a rapidly growing cutaneous angiosarcoma. Radiology did not show any signs of involvement of the lacrimal duct, metastasis, or local invasion or bone destruction. The tumor was surgically excised, as part of an exenteration procedure, and sent for histopathological examination. The defect was covered with a partial skin graft from the thigh. The histopathological examination confirmed radical removal of a 25 mm angiosarcoma. The narrowest margin was only 0.38 mm and the patient therefore underwent radiation therapy post-operatively.

### Study protocol

LSCI and HSI were performed *in vivo*, before tumor removal. PAI was applied *ex vivo*, on the excised tumor, within one hour after surgery. PAI was only performed *ex vivo* because it is currently not approved for *in vivo* imaging close to any of the eyes, due to laser safety considerations. After completion of the study protocol, the tumor was placed in formalin and sent for routine histopathological examination. [Figure 1](#) provides a schematic of the measurement geometries of all the imaging modalities in relation to the tissue.

### Laser speckle contrast imaging

Blood perfusion was monitored using a PeriCam LSCI instrument (PeriCam PSI NR System, Perimed AB, Stockholm, Sweden). The area of interest was illuminated with NIR laser light at a wavelength of 785 nm. The speckle pattern was recorded in real time by a camera, at a rate of up to 100 images per second, and a spatial resolution of 100  $\mu\text{m}/\text{pixel}$ . Perfusion was automatically calculated by the system by analyzing the

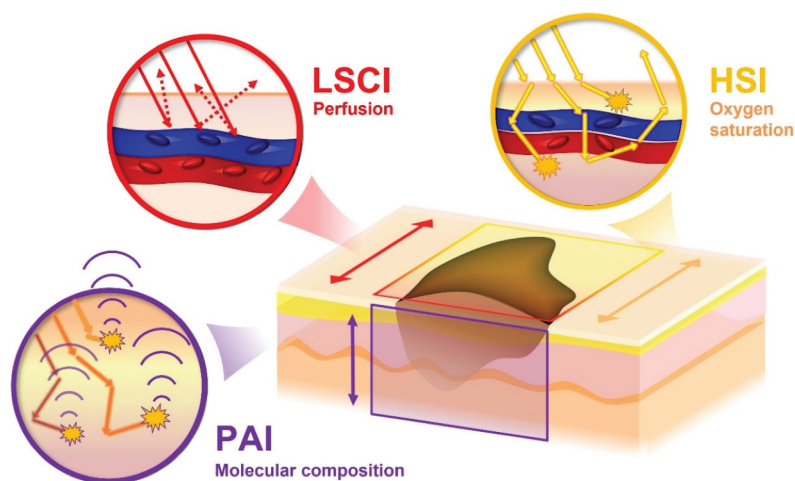


**Figure 1.** Schematic illustration of the combination of imaging modalities in the present study. Laser speckle (LSCI) and hyperspectral imaging (HSI), being so-called “light in – light out” techniques, provide 2D maps of the surface capable of depicting the tumor blood perfusion and oxygen saturation respectively. Photoacoustic imaging (PAI), a “light in – sound out” technique, can provide 3D maps of the molecular properties of tumor. The combination of techniques thereby has the capacity to provide detailed information of the functional and molecular properties of tumors useful in preoperative assessment.

variations in the speckle pattern. LSCI measures blood perfusion in arbitrary units, called perfusion units (PU).

### Hyperspectral imaging

HSI was performed using a custom-built push-broom camera from the HySpex series (Norsk Elektro Teknisk AS, Oslo, Norway). This type of HSI camera operates by illuminating the surface of the tissue with light emitted from a halogen lamp after which diffusely backscattered light is detected along a single line where a detailed spectrum is generated at every single point along the line. The light source and detector are fixed together and scan across the surface from which detailed spectral information is obtained across a larger area. The benefit of this type of HSI scanning is that the spectral information is more reliable and less prone to be affected by patient motion.

The spectral range of the camera is 400 to 1700 nm, divided into 382 spectral channels, yielding a spectral resolution of 3.4 nm. For the sake of avoiding overlapping signals from higher diffraction orders, the acquisition spectral range used in the study was limited to 600–1000 nm. The spatial resolution of the camera is on the order of 150  $\mu\text{m}/\text{pixel}$ , with a swath width of around 10 cm. A halogen light source operating at a temperature of 2900 K was used to provide white light illumination through a line-light generator that was aligned in order to overlap with the detection line of the camera. Both the camera and light source were placed on a linear translation stage with a total scanning distance of 25 cm. The scan speed was adjusted to match the exposure time of the camera (20 ms) such that consecutively acquired lines represent adjacent regions of

the object that are neither overlapping, nor separated in space. The entire scan, covering an area of  $10 \times 10 \text{ cm}^2$ , took roughly 15 seconds to complete. Further details concerning the technical aspects of the camera and acquisition procedure can be found elsewhere.<sup>12</sup>

The equipment was mounted on a movable arm on a trolley, allowing it to be easily positioned above the patient for *in vivo* scanning. The hyperspectral camera was placed 30 cm directly above the patient. The patient was specifically asked not to move during the measurement procedure, and the examiner paid special attention to this. A live view of the acquired data enabled quick visual assessment of image quality, which aided in determining whether the measurement needed to be repeated. During measurements, the lights in the room were dimmed to reduce background light.

The data produced by the HSI camera require processing before it can be further analyzed, as described in our previous study.<sup>12</sup> In essence, light diffusely reflected back from a white reference is used to normalize the detected light from the tissue surface from which the fraction of the light absorbed in the tissue can be determined.

### Photoacoustic imaging

PAI was performed using the Vevo LAZR-X imaging system (FUJIFILM Visualsonics, Toronto, Canada). During PAI, diagnostic ultrasound scans are interleaved with the laser pulses. In this system, an ultrasound transducer and a fiberoptic bundle were coupled to a 20 Hz tunable laser with a nanosecond pulse duration. The laser wavelength range used in this study was 680–970 nm. Two planar light

beams, located on either side of the ultrasound linear array, illuminate the skin surface. Each image was captured at 59 excitation wavelengths within the spectral range in steps of 5 nm. In the resulting multispectral image, each pixel therefore contained a single spectrum with 59 spectral components. The transducer and laser fibers were attached to a linear stepper motor to allow a sequence of multispectral photoacoustic images to be collected with a 0.5 mm step between each image. To prevent motion artifacts caused by the examiner, the transducer and stepper motor were attached to an adjustable arm (Mounting Accessory, GCX Corporation, Petaluma, CA, USA). Further details concerning the instrument and acquisition procedure can be found in our previous study.<sup>23</sup>

The excised tumor was mounted in a 100 × 70 × 50 mm custom-made Plexiglas container, containing isotonic saline solution, using 1–2 Prolene 6–0 sutures (Ethicon, Bridgewater, NJ, USA) at each end of the lesion. A layer of black ultrasound-attenuating material was placed in the bottom of the container. A 10 mm thick Aquaflex® Ultrasound gel pad (Parker Laboratories Inc., Fairfield, CT, USA) with protective plastic was used to achieve an adequate distance between the laser fibers and the tissue surface.

### Spectral unmixing

To interpret the spectral information obtained from each pixel in both the photoacoustic and hyperspectral images we employed a method called spectral unmixing. This method takes a single measured absorption spectrum and finds the optimal linear combination of other absorption spectra (or so-called endmember

spectra) that is required to best reproduce the measured spectrum. These endmember spectra represent known tissue chromophores, such as melanin, HbO<sub>2</sub> and HbR, collagen, fat, and water. Using a non-negative matrix factorization approach, as described previously,<sup>24</sup> linear coefficients representing the relative amount of each endmember can be extracted from which a comparison can be made. Spectral unmixing can therefore provide insight into the molecular composition of the examined tissue. It should be noted that the extracted information does not yield any quantifiable information, which is a limiting factor when it is necessary to extract concentrations of various tissue constituents. However, this is not a problem when determining the oxygen saturation, since this is a measure of the oxygenated hemoglobin in relation to the total Hb (HbT = HbO<sub>2</sub> + HbR). The use of spectral unmixing to extract oxygen saturation from PAI data has been described by us previously.<sup>24</sup>

## Results

### Laser speckle contrast imaging for perfusion monitoring

LSCI was first performed on the angiosarcoma *in vivo*. A perfusion map was obtained in which the perfusion ranged from 25 PU in the surrounding healthy skin, to 1100 PU at the center of the tumor (Figure 2), indicating a considerable increase in perfusion in the tumor as the result of the high vascularity. From the intensity map, the location of the angiosarcoma around the periorbital region is clear, providing some reference to how much

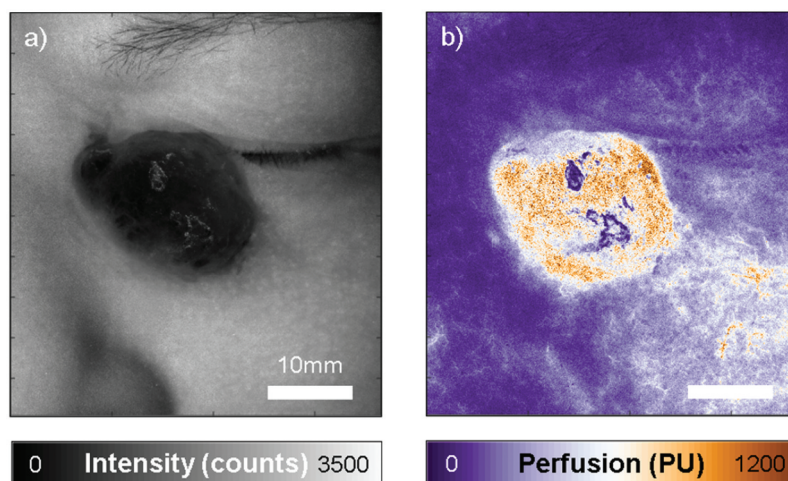


**Figure 2.** Laser speckle contrast imaging of the angiosarcoma, showing an intensity map on the left (a), and the corresponding perfusion map on the right (b). Perfusion in the tumor is markedly higher than in the surrounding skin. Perfusion and intensity are expressed in arbitrary units, intensity counts and perfusion units (PU). Both images are scaled the same and the scale bar represents 10mm.

the perfusion has increased in the tumor compared to what is normally a well perfused region.

### Hyperspectral imaging for oxygen saturation mapping

HSI was performed *in vivo* to map the oxygen saturation in the angiosarcoma (Figure 3A). The absorbance spectra were recorded in each pixel in the spectral range 600–1000 nm. However, due to the drastic drop in hemoglobin absorption between 600–700 nm, we limited the analysis to the 700–1000 nm spectral range. The spectra acquired from healthy skin differed from those acquired from the tumor (Figure 3B), indicating differences in the molecular composition. A change in spectral features was observed at both short and long wavelengths.

To gain insight into the molecular composition, spectral unmixing was performed using the endmembers melanin, HbO<sub>2</sub> and HbR, collagen, fat, and water. We first determined that the total hemoglobin (HbT = HbR+HbO<sub>2</sub>) was significantly higher in the tumor than in the surrounding skin (Figure 3C).

Thereafter, we were able to calculate the oxygen saturation and found that it was lower in the tumor than in the surrounding skin (Figure 3D). These results may be explained by the pooling of deoxygenated blood (HbR) in the angiosarcoma.

### Photoacoustic imaging for depth resolved molecular composition

Finally, PAI was performed *ex vivo* on the excised angiosarcoma. Spectral unmixing of the multiwavelength 3D scans provided a visual representation of the tumor in three dimensions, and enabled mapping of the relative contributions of the endmembers melanin, HbO<sub>2</sub> and HbR, collagen, fat, and water (Figure 4). The spectrum acquired from the tumor differed from that of healthy skin in that HbT increased and oxygen saturation decreased, which is in line with the results obtained from HSI, suggesting pooling of deoxygenated blood (HbR) in the angiosarcoma (Figure 4A and B). HSI shows the 2D distribution of chromophores on the skin surface, while PAI provides a 3D image. Figure 4C shows the distribution of HbO<sub>2</sub>, HbR, and collagen

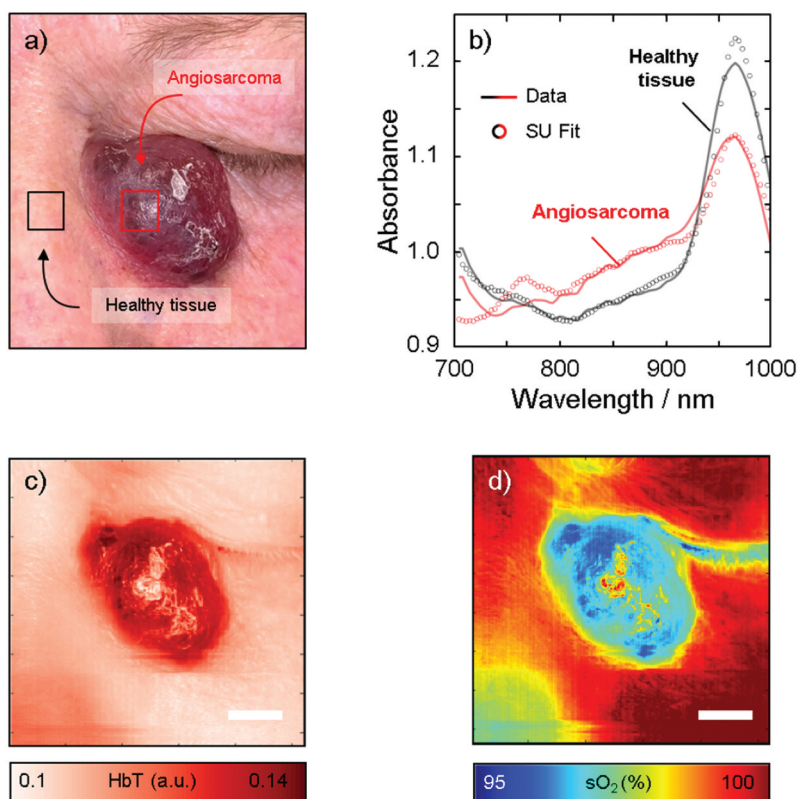


**Figure 3.** Hyperspectral imaging of the angiosarcoma *in vivo* with the corresponding photograph (a). The spectra in the tumor and the healthy skin shown in (b) were analyzed in the two regions of interest indicated by the red and black squares in (a). The solid lines indicate the measured spectra and the circles indicate the fit obtained by spectral unmixing (SU) of the measured spectra using the endmembers melanin, HbO<sub>2</sub> and HbR, collagen, fat, and water. From the spectral unmixing, we calculate HbT (c) and sO<sub>2</sub> (d). Note the increase in HbT and decrease in sO<sub>2</sub> in the tumor, suggesting the pooling of deoxygenated blood. Scale bar represents 10mm.

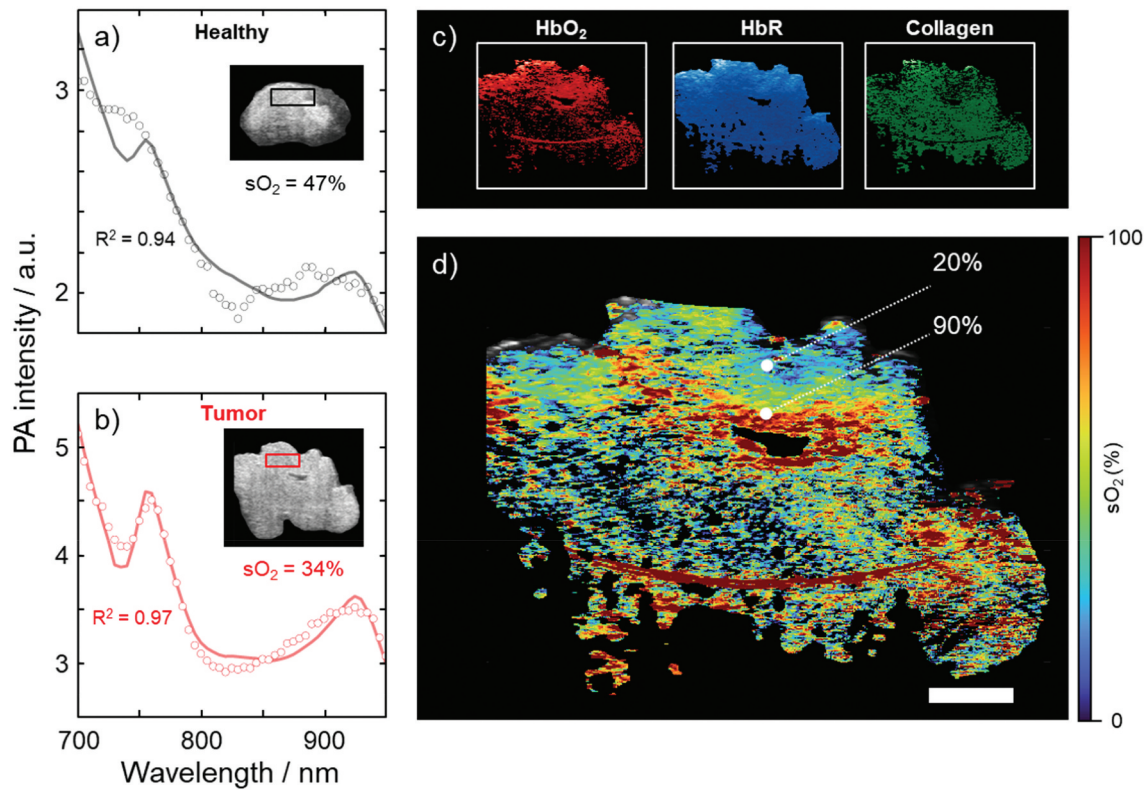


**Figure 4.** Results of photoacoustic imaging of the angiosarcoma, *ex vivo*. The spectra in healthy tissue (a) and the tumor (b) were analyzed in the two regions of interest (black and red squares, respectively) indicated in the inset cross-sectional ultrasound images. Spectral unmixing was performed to obtain maps of the relative contributions of the endmembers HbO<sub>2</sub>, HbR, and collagen (c), from which an oxygen saturation map was generated (d), according to the method outlined above. Scale bar represents 10 mm. R<sup>2</sup> represents the coefficient of determination indicating how well the spectral unmixing model fits the data.

throughout the tumor, of which the first two could be used to calculate the oxygen saturation as a function of depth (Figure 4D).

## Discussion

This is the first study to be performed on the combination of three emerging non-invasive medical imaging techniques, LSCI, HSI, and PAI, to image a skin tumor. Two-dimensional maps of perfusion and oxygen saturation were obtained using LSCI and HSI respectively, together with 3D maps of the molecular composition of the tumor, obtained by PAI. We have previously demonstrated the benefit of combining LSCI and HSI during reconstructive flap surgery, highlighting the fact that perfusion and oxygenation do not necessarily act in direct unison.<sup>11</sup> In the present study, we have demonstrated that an increase in perfusion does not necessarily equate with an increase in oxygen saturation, as may be assumed. PAI provides information as a function of depth in the tumor, which enables additional clinical applications where non-invasive

diagnostics is of importance. Apart from skin tumor diagnostics, PAI has been used in several clinical applications, oxygen saturation monitoring being one of the more common.<sup>25</sup> In this study, we also highlight the additional information that can be obtained using spectral unmixing to characterize the molecular composition of tissue in three dimensions, which could be useful in comprehensive mapping for preoperative assessment of tumors in the future.

## Combined technology

The combination of all three imaging modalities exploits the two fundamental light – matter interactions, namely, scattering and absorption, and their interaction in tissue. LSCI makes direct use of diffusely scattered light, from which perfusion can be determined. HSI also makes use of diffusely scattered light, but the absorption of photons in the tissue is obtained indirectly by relating the number of photons entering the tissue to those leaving the tissue. PAI, on the other hand, measures light absorption in tissue more directly, while also providing depth-resolved information. While HSI and PAI

are based on absorption, scattering is indirectly a necessary component for both imaging modalities as it to a degree assists the passage of light through the examined tissue and allows for the tissue to be examined from the surface, which in turn enables non-invasive diagnostics. Furthermore, while HSI and PAI both provide information on absorption, they are complementary in the sense that they provide a spatially resolved picture on the tissue surface (i.e. 2D), and as a function of depth (3D), respectively.

### **LSCI reveals increased perfusion in angiosarcoma**

LSCI revealed increased perfusion in this tumor, interpreted as increased vascularity, which is a hallmark of angiosarcoma. This is in line with a previous study on cherry angiomas in humans showing increased perfusion, describing this highly vascularized tumor.<sup>10</sup> LSCI has hitherto only rarely been applied in conjunction with skin tumors. Linkous et al. imaged malignant melanoma, but instead found increased perfusion around the periphery of the lesion, and lower perfusion centrally over the lesion, which they explained by the mass of proliferating melanocytes with inadequate vascularization.<sup>26</sup> Further studies on LSCI mapping of the vascularity of skin tumors may aid in the preoperative assessment.

### **Assessing oxygen saturation from the surface**

HSI enabled detailed 2D mapping of spectral features on the surface of the tumor. The conventional spectroscopic approach for assessing  $sO_2$  is to analyze only the spectral signatures of  $HbO_2$  and  $HbR$ . Despite being the strongest light absorbers in tissue,  $HbO_2$  and  $HbR$  are not the only tissue components that can be effectively measured with optical techniques. Bickler et al. found that the accuracy in  $sO_2$  decreased at lower values of  $sO_2$  in subjects with dark skin, due to the increased melanin content,<sup>27</sup> which has been emphasized in a recent communication.<sup>28</sup> We have recently employed a technique for improving the accuracy of  $sO_2$  mapping by spectral unmixing using multiple light-absorbing tissue components.<sup>12</sup> In the present study, spectral unmixing was employed using the endmembers melanin, water, collagen, and fat to provide accurate measurements of  $HbT$  and  $sO_2$ . The results showed clinically relevant oxygen saturation levels around 98% in healthy tissue. In the angiosarcoma, total hemoglobin was markedly higher, while oxygen saturation was found to be lower, which may be explained by the pooling of deoxygenated blood ( $HbR$ ), which is in line with its clinical vascularization features.

HSI has recently gained attention as a non-invasive tool for oncologists when assessing tumor characteristics and tumor burden, and a growing number of reports demonstrate its application to human skin tumors.<sup>29</sup> Most previous studies employing spectral imaging for skin tumor diagnosis and delineation have mainly focused on melanomas, and whether or not they can be distinguished from benign skin tumors using spectral information. One study employing multispectral imaging reported a specificity of 67% and a sensitivity of 25%.<sup>30</sup> Others have reported higher sensitivity, from 80 to 100%, and specificity from 76% to 89%.<sup>31–33</sup> However, studies using HSI with several spectral bands have shown the most promising results. A research group in Japan has developed an algorithm for HSI analysis that can distinguish melanomas from other pigmented skin lesions with a sensitivity and specificity of 96% and 97%, respectively<sup>34</sup>; outperforming dermatoscope-aided examinations.

### **PAI depicts the chromophoric composition as a function of depth**

The added value of PAI imaging over HSI is its potential to map spectral features as a function of depth to provide a 3D image of the endogenous chromophores in the tissue. PAI therefore has potential for the non-invasive preoperative delineation of skin tumors in 3D. In the present study, PAI was used for the first time for the 3D spectral mapping of an angiosarcoma.

Encouraging results have previously been obtained with PAI in animal studies, showing that it could be developed into a tool for the non-invasive diagnosis of malignant melanoma.<sup>35–39</sup> Only a few studies have been performed on human skin cancer, most of which were on melanotic skin tumors,<sup>35,36,38–49</sup> and only a few on non-melanotic skin tumors.<sup>49–51</sup> We recently reported on a case of skin cancer in which PAI was suggested as an alternative technique for intraoperative micrographic control of the surgical margins on the eyelid.<sup>52</sup>

In the present study, 59 wavelengths were used over a broader spectral range (680–970 nm), to provide more detailed information on the molecular composition of the tissue, thus increasing the probability of identifying differences between tumor and healthy tissue. In a recent study on 52 melanomas,<sup>23</sup> our group was able to show that using more excitation wavelengths allowed for more robust spectral unmixing analysis, providing a more detailed map of the distribution of tumor cells, compared to the use of only a few wavelengths. This constitutes a distinct improvement on the previous studies mentioned above, in which tumor borders were defined only by high absorption amplitudes or by the photoacoustic absorption signal of melanin alone.

We also used multiple wavelengths to allow for detailed spectral unmixing analysis with regard to melanin, HbO<sub>2</sub> and HbR, collagen, fat, and water. The results showed the spectral features that would be expected for an angiosarcoma, being a malignant tumor originating from lymphatic or vascular endothelial cells.<sup>53</sup> The cherry red color of the tumor is due to pooling of deoxygenated hemoglobin, as shown by the increase in total hemoglobin and decrease in sO<sub>2</sub>. The tumor disrupts the tissue-supporting structures, resulting in a decrease in the collagen content and lower melanin content.

In the present case, the borders of the angiosarcoma were clearly visible to the bare eye. Indeed, this is a proof-of-concept study and imaging would probably not change much of the surgical procedure in the present case. The benefit of using pre-operative bioimaging techniques in the future lies in tumors with borders that are difficult to define. A larger comparative study must be undertaken before any conclusions can be drawn regarding tumor margins assessment by imaging vs. clinically.

### **Laser safety in the periorbital area**

PAI was only performed *ex vivo* after tumor excision, due to laser safety considerations. It is important to prevent strong light from entering the eye via the focusing structures, i.e. the cornea and lens, and reaching the choroid, which contains melanin that exhibits significant light absorption in the PAI excitation range (680–970 nm). The implementation of appropriate safety precautions may allow PAI to be used for imaging in the vicinity of the eye in the future. However, scattering is still relevant in the wavelength region of interest, causing the propagating light, and its energy, to be rapidly spread over a large volume. Thus, any light indirectly entering the eye via the sclera would be highly scattered and unfocused. However, this needs to be tested before any further conclusions on the safe use of PAI can be made. Despite current safety concerns regarding *in vivo* examinations, we believe that PAI imaging could be developed to assist in intraoperative micrographic control of the surgical margins. Freshly excised tumors can be scanned rapidly to determine whether excision is indeed radical, or if further excision is necessary. This would lead to considerable savings in both time and resources compared to conventional microscopic histology as in Mohs micrographic surgery.

### **Conclusion**

In conclusion, this proof-of-principle study has demonstrated the feasibility of combining LSCI, HSI, and PAI to provide detailed maps of the functional and molecular properties of tumors in 3D.

Multiwavelength 3D scanning and spectral unmixing provided distributions of the endmembers melanin, HbO<sub>2</sub>, HbR and collagen in the overall tumor architecture. The present study was performed on a rapidly growing and invasive angiosarcoma. Further studies are needed for testing the applicability in less aggressive, less vascular lesions, such as basal cell carcinoma and squamous cell carcinoma. Furthermore, the diagnostic sensitivity of this combination of techniques needs to be further evaluated in a larger number of patients before they can be introduced in clinical practice.

### **Acknowledgment**

The authors express their gratitude to John Albinsson for his assistance during the measurements. This study was supported by the Swedish Cancer Foundation, Berta Kamprad's Foundation, the Sjöberg Foundation, Lund University grant for Research Infrastructure, the Swedish Government Grant for Clinical Research (ALF), Skåne University Hospital (SUS) Research Grants, Skåne County Council Research Grants, Crown Princess Margaret's Foundation (KMA), Friends of the Visually Impaired Association in the county of Gävleborg, the Foundation for the Visually Impaired in the County of Malmöhus, Carmen and Bertil Regné's Foundation, IngaBritt and Arne Lundberg's Research Foundation, the Swedish Eye Foundation, the Cronqvist Foundation and the Swedish Medical Association.

### **Disclosure statement**

The authors report no conflicts of interest. The authors alone are responsible for the content and writing of the article.

### **Funding**

This study was supported by the Knut and Alice Wallenberg Foundation to SciLifeLab for research in Data-driven Life Science, DDLS (KAW 2020.0239), the Swedish Cancer Foundation, Mrs Berta Kamprad Foundation, the Sjöberg Foundation, Lund University grant for Research Infrastructure, the Swedish Government Grant for Clinical Research (ALF), Skåne University Hospital (SUS) Research Grants, Skåne County Council Research Grants, Crown Princess Margaret's Foundation (KMA), Friends of the Visually Impaired Association in the county of Gävleborg, the Foundation for the Visually Impaired in the County of Malmöhus, Carmen and Bertil Regné Foundation, IngaBritt and Arne Lundberg's Research Foundation, the Swedish Eye Foundation, Cronqvist Foundation, Swedish Medical Association, and the Edvin Giströms Foundation.

### **ORCID**

Magne Stridh  <http://orcid.org/0000-0003-3395-3273>

Ulf Dahlstrand  <http://orcid.org/0000-0002-6843-7896>  
 Magdalena Naumovska  <http://orcid.org/0000-0003-0015-7326>

Karl Engelsberg  <http://orcid.org/0000-0001-7951-5709>

Rafi Sheikh  <http://orcid.org/0000-0002-8289-9114>

Aboma Merdasa  <http://orcid.org/0000-0002-6298-5672>

Malin Malmsjö  <http://orcid.org/0000-0001-9849-9599>

## References

1. *Clinical practice guidelines for keratinocyte cancer*. Cancer Council Australia Keratinocyte Cancers Guideline Working Party 2029-11-07 2023-10-04. <https://www.cancer.org.au/clinical-guidelines/skin-cancer/keratinocyte-cancer>.
2. *Clinical practice guidelines for the diagnosis and management of melanoma*. Cancer Council Australia Melanoma Guidelines Working Party. 2021-04-22 2023-10-04. <https://www.cancer.org.au/clinical-guidelines/skin-cancer/melanoma>.
3. Ferrante di Ruffano L, Dinnes J, Deeks J, Chuchu N, Bayliss S, Davenport C, et al. Optical coherence tomography for diagnosing skin cancer in adults. *Cochrane Database Syst Rev*. 2018;12(12):CD013189. doi:10.1002/14651858.CD013189.
4. Sahu A, Oh Y, Cordova M, Navarrente-Dechent C, Gill M, Alessi-Fox C, et al. In vivo optical imaging-guided targeted sampling for precise diagnosis and molecular pathology. *Sci Rep*. 2021;11(1):23124. doi:10.1038/s41598-021-01447-4.
5. Wielowieyska-Szybinska D, Bialek-Galas K, Podolec K, Wojas-Pelc A. The use of reflectance confocal microscopy for examination of benign and malignant skin tumors. *Postepy Dermatol Alergol*. 2014;31(6):380–387. doi:10.5114/pdia.2014.40961.
6. Chen HY, Wilson CB, Tycko R. Enhanced spatial resolution in magnetic resonance imaging by dynamic nuclear polarization at 5 K. *Proc Natl Acad Sci USA*. 2022;119(22):e2201644119. doi:10.1073/pnas.2201644119.
7. Yamamoto Y, Ohura T, Nohira K, Sugihara T, Minakawa H, Igawa H, et al. Laserflowgraphy: a new visual blood flow meter utilizing a dynamic laser speckle effect. *Plast Reconstr Surg*. 1993;91(5):884–894. doi:10.1097/00006534-199304001-00022.
8. Berggren J, Castelo N, Tenland K, Dahlstrand U, Engelsberg K, Lindstedt S, et al. Reperfusion of free full-thickness skin grafts in periocular reconstructive surgery monitored using laser speckle contrast imaging. *Ophthalmic Plast Reconstr Surg*. 2021;37(4):324–328. doi:10.1097/IOP.0000000000001851.
9. Berggren J, Castelo N, Tenland K, Dahlstrand U, Engelsberg K, Lindstedt S, et al. Revascularization of free skin grafts overlying modified Hughes tarsoconjunctival flaps monitored using laser-based techniques. *Ophthalmic Plast Reconstr Surg*. 2019;35(4):378–382. doi:10.1097/IOP.0000000000001286.
10. Linkous C, Pagan A, Shope C, Andrews L, Snyder A, Ye T, et al. Applications of laser speckle contrast imaging technology in dermatology. *JID Innov*. 2023;3(5):100187. doi:10.1016/j.xjidi.2023.100187.
11. Bunke J, Merdasa A, Stridh M, Rosenquist P, Berggren J, Hernandez-Palacios J, et al. Hyperspectral and laser speckle contrast imaging for monitoring the effect of epinephrine in local anesthetics in oculoplastic surgery. *Ophthalmic Plast Reconstr Surg*. 2022;38(5):462–468. doi:10.1097/IOP.0000000000002163.
12. Merdasa A, Berggren J, Tenland K, Stridh M, Hernandez-Palacios J, Gustafsson N, et al. Oxygen saturation mapping during reconstructive surgery of human forehead flaps with hyperspectral imaging and spectral unmixing. *Microvasc Res*. 2023;150:104573. doi:10.1016/j.mvr.2023.104573.
13. Leon R, Martinez-Vega B, Fabelo H, Ortega S, Melian V, Castaño I, et al. Non-invasive skin cancer diagnosis using hyperspectral imaging for in-situ clinical support. *JCM*. 2020;9(6):1662. doi:10.3390/jcm9061662.
14. Chin MS, Freniere BB, Lancerotto L, Lujan-Hernandez J, Saleeby JH, Lo Y-C, et al. Hyperspectral imaging as an early biomarker for radiation exposure and microcirculatory damage. *Front Oncol*. 2015;5:232. doi:10.3389/fonc.2015.00232.
15. Chin MS, Babchenko O, Lujan-Hernandez J, Nobel L, Ignatz R, Lalikos JF. Hyperspectral imaging for burn depth assessment in an animal model. *Plast Reconstr Surg Glob Open*. 2015;3(12):e591. doi:10.1097/GOX.0000000000000558.
16. Sowa MG, Payette JR, Hewko MD, Mantsch HH. Visible-near infrared multispectral imaging of the rat dorsal skin flap. *J Biomed Opt*. 1999;4(4):474–481. doi:10.1117/1.429957.
17. Khaodhiar L, Dinh T, Schomacker KT, Panasyuk SV, Freeman JE, Lew R, et al. The use of medical hyperspectral technology to evaluate microcirculatory changes in diabetic foot ulcers and to predict clinical outcomes. *Diab Care*. 2007;30(4):903–10. doi:10.2337/dc06-2209.
18. Nouvong A, Hoogwerf B, Mohler E, Davis B, Tajaddini A, Medenilla E. Evaluation of diabetic foot ulcer healing with hyperspectral imaging of oxyhemoglobin and deoxyhemoglobin. *Diab Care*. 2009;32(11):2056–61. doi:10.2337/dc08-2246.
19. Chiang N, Jain JK, Sleigh J, Vasudevan T. Evaluation of hyperspectral imaging technology in patients with peripheral vascular disease. *J Vasc Surg*. 2017;66(4):1192–1201. doi:10.1016/j.jvs.2017.02.047.
20. Goetze E, Thiem D, Gielisch MW, Kämmerer PW. Identification of cutaneous perforators for microvascular surgery using hyperspectral technique - a feasibility study on the antero-lateral thigh. *J Craniomaxillofac Surg*. 2020;48(11):1066–1073. doi:10.1016/j.jcms.2020.09.005.
21. Lin L, Wang LV. The emerging role of photoacoustic imaging in clinical oncology. *Nat Rev Clin Oncol*. 2022;19(6):365–384. doi:10.1038/s41571-022-00615-3.
22. Stridh MT, Hult J, Merdasa A, Albinsson J, Pekar-Lukacs A, Gesslein B, et al. Photoacoustic imaging of periorbital skin cancer ex vivo: unique spectral signatures of malignant melanoma, basal, and squamous cell carcinoma. *Biomed Opt Express*. 2022;13(1):410–425. doi:10.1364/BOE.443699.
23. Hult J, Merdasa A, Pekar-Lukacs A, Tordengren M, Khodaverdi A, Albinsson J, et al. Comparison of photoacoustic imaging and histopathological examination in

- determining the dimensions of 52 human melanomas and nevi ex vivo. *Biomed Opt Express*. 2021;12(7):4097–4114. doi:10.1364/BOE.425524.
24. Merdasa A, Bunke J, Naumovska M, Albinsson J, Erlöv T, Cinthio M, et al. Photoacoustic imaging of the spatial distribution of oxygen saturation in an ischemia-reperfusion model in humans. *Biomed Opt Express*. 2021;12(4):2484–2495. doi:10.1364/BOE.418397.
  25. Attia ABE, Balasundaram G, Moothanchery M, Dinesh US, Bi R, Ntziachristos V, et al. A review of clinical photoacoustic imaging: Current and future trends. *Photoacoustics*. 2019;16:100144. doi:10.1016/j.pacs.2019.100144.
  26. Kontos CD. More than skin deep: connecting melanocyte pigmentation and angiogenic diseases. *J Clin Invest*. 2014;124(1):76–9. doi:10.1172/JCI73559.
  27. Bickler PE, Feiner JR, Severinghaus JW. Effects of skin pigmentation on pulse oximeter accuracy at low saturation. *Anesthesiology*. 2005;102(4):715–719. doi:10.1097/0000542-200504000-00004.
  28. Keller MD, Harrison-Smith B, Patil C, Arefin MS. Skin colour affects the accuracy of medical oxygen sensors. *Nature*. 2022;610(7932):449–451. doi:10.1038/d41586-022-03161-1.
  29. Alopogianni E, Ishikawa M, Kobayashi N, Obi T. Hyperspectral and multispectral image processing for gross-level tumor detection in skin lesions: a systematic review. *J Biomed Opt*. 2022;27(6). doi:10.1117/1.JBO.27.6.060901.
  30. Song E, Grant-Kels JM, Swede H, D'Antonio JL, Lachane A, Dadras SS, et al. Paired comparison of the sensitivity and specificity of multispectral digital skin lesion analysis and reflectance confocal microscopy in the detection of melanoma in vivo: a cross-sectional study. *J Am Acad Dermatol*. 2016;75(6):1187–1192.e2. doi:10.1016/j.jaad.2016.07.022.
  31. Lorencs A, Sinavskis-Sinica J, Jakovels D, Mednieks I. Melanoma-nevus discrimination based on image statistics in few spectral channels. *Elektronika ir Elektrotechnika*. 2016;22(2):66–72. doi:10.5755/j01.eie.22.2.14594.
  32. Thomas L, Puig S. Dermoscopy, digital dermoscopy and other diagnostic tools in the early detection of melanoma and follow-up of high-risk skin cancer patients. *Acta Derm Venereol*. 2017;Suppl 218:14–21. doi:10.2340/00015555-2719.
  33. Carrara M, Bono A, Bartoli C, Colombo A, Lualdi M, Moglia D, et al. Multispectral imaging and artificial neural network: mimicking the management decision of the clinician facing pigmented skin lesions. *Phys Med Biol*. 2007;52(9):2599–613. doi:10.1088/0031-9155/52/9/018.
  34. Nagaoka T, Kiyohara Y, Koga H, Nakamura A, Saida T, Sota T. Modification of a melanoma discrimination index derived from hyperspectral data: a clinical trial conducted in 2 centers between March 2011 and December 2013. *Skin Res Technol*. 2015;21(3):278–283. doi:10.1111/srt.12188.
  35. Oh JT, Li M-L, Zhang HF, Maslov K, Stoica G, Wang LV. Three-dimensional imaging of skin melanoma in vivo by dual-wavelength photoacoustic microscopy. *J Biomed Opt*. 2006;11(3):34032. doi:10.1117/1.2210907.
  36. Wang Y, Xu D, Yang S, Xing D. Toward in vivo biopsy of melanoma based on photoacoustic and ultrasound dual imaging with an integrated detector. *Biomed Opt Express*. 2016;7(2):279–286. doi:10.1364/BOE.7.000279.
  37. Zhou Y, Li G, Zhu L, Li C, Cornelius LA, Wang LV. Handheld photoacoustic probe to detect both melanoma depth and volume at high speed in vivo. *J Biophotonics*. 2015;8(11–12):961–967. doi:10.1002/jbio.201400143.
  38. Zhou Y, Xing W, Maslov KI, Cornelius LA, Wang LV. Handheld photoacoustic microscopy to detect melanoma depth in vivo. *Opt Lett*. 2014;39(16):4731–4734. doi:10.1364/OL.39.004731.
  39. Zhou Y, Tripathi SV, Rosman I, Ma J, Hai P, Linette GP, et al. Noninvasive determination of melanoma depth using a handheld photoacoustic probe. *J Invest Dermatol*. 2017;137(6):1370–1372. doi:10.1016/j.jid.2017.01.016.
  40. Malvey J, Pellacani G. Dermoscopy, confocal microscopy and other non-invasive tools for the diagnosis of non-melanoma skin cancers and other skin conditions. *Acta Derm Venereol*. 2017;Suppl 218:22–30. doi:10.2340/00015555-2720.
  41. Smith L, MacNeil S. State of the art in non-invasive imaging of cutaneous melanoma. *Skin Res Technol*. 2011;17(3):257–269. doi:10.1111/j.1600-0846.2011.00503.x.
  42. Kim C, Erpelding TN, Jankovic L, Pashley MD, Wang LV. Deeply penetrating in vivo photoacoustic imaging using a clinical ultrasound array system. *Biomed Opt Express*. 2010;1(1):278–284. doi:10.1364/BOE.1.000278.
  43. Lin L, Hu P, Shi J, Appleton CM, Maslov K, Li L, et al. Single-breath-hold photoacoustic computed tomography of the breast. *Nat Commun*. 2018;9(1):2352. doi:10.1038/s41467-018-04576-z.
  44. Yao J, Wang LV. Photoacoustic tomography: fundamentals, advances and prospects. *Contrast Media Mol Imaging*. 2011;6(5):332–345. doi:10.1002/cmimi.443.
  45. Brethnach A, Concannon E, Dorairaj JJ, Shaharan S, McGrath J, Jose J, et al. Preoperative measurement of cutaneous melanoma and nevi thickness with photoacoustic imaging. *J Med Imaging (Bellingham)*. 2018;5(1):015004. doi:10.1117/1.JMI.5.1.015004.
  46. Brethnach A, Concannon L, Aalto L, Dorairaj J, Subhash HM, Kelly J, et al. Assessment of cutaneous melanoma and pigmented skin lesions with photoacoustic imaging. In: Kang HW, Wong BJJ, Ilgner JF, Nuttall AL, Richter CP, Skala MC, et al., eds. *Proc SPIE, Photonic Therapeutics and Diagnostics XI*. Vol. 9303. San Francisco, CA: SPIE; 2015:930303.
  47. Valluru KS, Wilson KE, Willmann JK. Photoacoustic imaging in oncology: translational preclinical and early clinical experience. *Radiology*. 2016;280(2):332–49. doi:10.1148/radiol.16151414.
  48. Kim J, Kim YH, Park B, Seo H-M, Bang CH, Park GS, et al. Multispectral ex vivo photoacoustic imaging of cutaneous melanoma for better selection of the excision margin. *Br J Dermatol*. 2018;179(3):780–782. doi:10.1111/bjd.16677.
  49. Chuah SY, Attia ABE, Long V, Ho CJH, Malempati P, Fu CY, et al. Structural and functional 3D mapping of skin tumours with non-invasive multispectral

- optoacoustic tomography. *Skin Res Technol.* 2017;23(2):221–226. doi:10.1111/srt.12326.
50. Attia ABE, Chuah SY, Razansky D, Ho CJH, Malempati P, Dinish US, et al. Noninvasive real-time characterization of non-melanoma skin cancers with handheld optoacoustic probes. *Photoacoustics.* 2017;7:20–26. doi:10.1016/j.pacs.2017.05.003.
51. Chuah SY, Attia ABE, Ho CJH, Li X, Lee J-S-S, Tan MWP, et al. Volumetric multispectral optoacoustic tomography for 3-dimensional reconstruction of skin tumors: a further evaluation with histopathologic correlation. *J Invest Dermatol.* 2019;139(2):481–485. doi:10.1016/j.jid.2018.08.014.
52. Dahlstrand U, Sheikh R, Malmsjo M. Photoacoustic imaging for intraoperative micrographic control of the surgical margins of eyelid tumours. *Acta Ophthalmol.* 2020;98(2):e264–e265. doi:10.1111/aos.14245.
53. Buehler D, Rice SR, Moody JS, Rush P, Hafez G-R, Attia S, et al. Angiosarcoma outcomes and prognostic factors: a 25-year single institution experience. *Am J Clin Oncol.* 2014;37(5):473–479. doi:10.1097/COC.0b013e31827e4e7b.